The Xe shielding surfaces for Xe interacting with linear molecules and spherical tops

Devin N. Sears and Cynthia J. Jameson
Department of Chemistry, M/C-111, University of Illinois at Chicago, Chicago, Illinois 60607-7061

(Received 9 February 2004; accepted 13 April 2004)

The ^{129}Xe nuclear magnetic resonance spectrum of xenon in gas mixtures of Xe with other molecules provides a test of the *ab initio* surfaces for the intermolecular shielding of Xe in the presence of the other molecule. We examine the electron correlation contributions to the Xe–CO_2, Xe–N_2, Xe–CO, Xe–CH_4, and Xe–CF_4 shielding surfaces and test the calculations against the experimental temperature dependence of the density coefficients of the Xe chemical shift in the gas mixtures at infinite dilution in Xe. Comparisons with the gas phase data permit the refinement of site–site potential functions for Xe–N_2, Xe–CO, and Xe–CF_4 especially for atom-Xe distances in the range 3.5–6 Å. With the atom–atom shielding surfaces and potential parameters obtained in the present work, construction of shielding surfaces and potentials for applications such as molecular dynamics averaging of Xe chemical shifts in liquid solvents containing CH_3, CH_2, CF_3, and CF_2 groups is possible. © *2004 American Institute of Physics.* [DOI: 10.1063/1.1758691]

INTRODUCTION

The range of Xe nuclear magnetic resonance (NMR) chemical shifts for Xe dissolved in organic solvents is of the order of 300 ppm, typical values are from 85 ppm in hexafluorobenzene, to 237 in methyl iodide and 245 ppm in dimethyl sulfoxide.[1,2] This large chemical shift range in solutions suggests an equally large range for Xe in solid materials. Xe atoms trapped in rigid inorganic crystals have been widely studied by NMR.[3] In polymers, Xe chemical shifts ranging from 83 ppm in poly(tetrafluoroethylene) to 220 ppm in polystyrene have been observed at room temperature.[4] There are, as yet, no comparable Xe NMR studies in solid biological systems, although peptide nanotubes offer interesting environments with one-dimensional channels analogous to aluminosilicates.[5,6] A renewed interest in the applications of Xe NMR as a probe of biological systems can be attributed to the increased sensitivity afforded by hyperpolarized ^{129}Xe.[7] Currently known Xe chemical shifts in the latter environments include 197 ppm in a lipid emulsion,[8] 216 ppm for Xe in red blood cells,[9] and 192 ppm in blood plasma.[9] These applications rely on the Xe shielding response to different electronic environments. Theoretical studies which contribute to our understanding of the Xe shielding response in simpler systems such as gas phase mixtures can be helpful in predicting Xe shielding response in complex electronic environments such as solutions or protein pockets.

Previous interpretations of Xe chemical shifts in solutions were empirically based, using refractive indices of the solvent as a means of correlating the chemical shifts.[10] Theoretical calculations of Xe chemical shifts in a liquid solvent would be possible by molecular dynamics simulations if the Xe chemical shift were known as a function of the coordinates of Xe and a solvent molecule cage. We have begun to use this approach, calculating the chemical shifts by *ab initio* and density functional methods for Xe in cages of 20 or more water molecules,[11] tested against experimental data for Xe in polycrystalline clathrate hydrates,[12–14] in preparation for calculating the average Xe chemical shift in liquid water via molecular dynamics.[15,16] The large difference in Xe chemical shifts in solution in alkanes vs fluoroalkanes is an intriguing observation. There are no comparable cages of crystalline alkanes or fluoroalkanes in which Xe can be trapped. Thus, we will use gas phase experiments to test the Xe shielding response calculations. Similarly, we have tested calculations of Xe chemical shift functions for Xe–CO_2, Xe–CO, and Xe–N_2 (Ref. 17) against the experimental density coefficients in these gases as a function of temperature, in the limit of infinite dilution in Xe.[18–20] In the present work, we repeat the latter calculations in order to take into account the electron correlation contributions to Xe chemical shifts that were missing from the earlier Hartree–Fock calculations. In this paper, we calculate the Xe shielding as a function of configuration in the supermolecular systems Xe–CH_4, Xe–CF_4 using Hartree–Fock and density functional methods, and in Xe–CO_2, Xe–CO, Xe–N_2 systems using density functional methods. By comparison with gas phase data, we obtain the parameters that will permit the construction of shielding surfaces and potentials for later applications to molecular dynamics averaging of Xe chemical shifts in liquid solvents containing CH_3, CH_2, CH, CF_3, CF_2, and CF groups.

APPROACH

We carry out Hartree–Fock and density functional calculations of Xe shielding in various configurations of the Xe–CO_2, Xe–CO, Xe–N_2, Xe–CH_4, and Xe–CF_4 supermolecular systems. The isotropic shielding is fitted to an appropriate functional form to reproduce the calculated values and also to provide interpolated values for arbitrary configurations. For Xe–CH_4 and Xe–CF_4, the form of the shielding function is taken to be of the pairwise additive site–site Xe–H, Xe–C, and Xe–F shielding functions, so that the lat-

ter can be used for Xe dissolved in alkanes and perfluoroalkanes. Potential functions describing the binary interactions are adopted for each system, using wherever possible, functions that have been fitted to van der Waals spectra and crossed molecular beam scattering data. The temperature dependent second virial coefficient $\sigma_1(T)$ of the Xe chemical shift in gas mixtures of Xe and CO_2, CO, N_2, CH_4, and CF_4 in the limit of zero mole fraction of Xe is calculated using the adopted potential functions, as follows:

$$\sigma_1(T) = \int\int\int \sigma(R,\theta,\phi)\exp[-V(R,\theta,\phi)/k_BT] \times R^2\, dR \sin\theta\, d\theta\, d\phi, \quad (1)$$

and compared with the published gas phase results. The resulting isotropic shielding functions $\sigma(R,\theta,\phi)$ and potential functions $V(R,\theta,\phi)$ can later be used for simulations involving solutions of Xe in liquid solvents containing CH_3, CH_2, CH, CF_3, CF_2, and CF groups, provided they can be written in terms of pairwise site–site forms.

SHIELDING CALCULATIONS AND SHIELDING FUNCTIONS

For Xe atom, we used 240 basis functions, an uncontracted $29s21p17d9f$ set that we have found to provide an accurate shielding response at various orientations and intermolecular separations. The core $(25s18p13d)$ was taken from Partridge and Faegri;[21] this was augmented by $3s$, $2p$, $4d$, and $9f$ orbitals with exponents taken from Bishop.[22] For C, N, O, F, and H, the Pople-type 6-311G** basis set was used.

For CH_4 and CF_4, three configurations were considered at various Xe–C separations: the first in which the Xe approach is collinear with the HC (or FC) bond, the second in which the Xe approach is perpendicular to the triangular face of the tetrahedral molecule, and the third in which the Xe approach is perpendicular to an edge of the tetrahedron. Since the Xe–CH_4 and Xe–CF_4 systems are to be used to generate useful functions that are transportable to liquid solvents containing CH_n and CF_n functional groups, the shielding values were fitted to site–site pairwise additive functions. We describe the calculated values for Xe shielding in the Xe–CH_4 and Xe–CF_4 systems using Xe–H, Xe–C, and Xe–F and Xe–C (which could be different from the other Xe–C) site–site functions of the internuclear separation, in the same functional form as the Xe–Rg (Rg = Xe,Kr,Ar,Ne) shielding functions:

$$\{\sigma(R,\theta,\phi)-\sigma(\infty)\} = \sum_{p=6,\text{even}}^{12} c_p R_{\text{XeC}}^{-p} + \sum_{i=1}^{4}\sum_{p=6,\text{even}}^{12} h_p R_{\text{Xei}}^{-p}, \quad (2)$$

where the coefficients c_p and h_p (or f_p) correspond to the site–site Xe–C and Xe–H (or Xe–C and Xe–F) shielding functions. We fit the Xe–CH_4 shielding values to Xe–C and Xe–H pairwise functions such as to have the *ab initio* values for the configuration with collinear Xe–H–C serve as the lower bounds for the Xe–H shielding function. Similarly, in the fitting to the Xe–CF_4 shielding values, the values for the configuration with collinear Xe–F–C were used as the lower bounds for the Xe–F shielding function. It turns out that the Xe–C shielding functions resulting from the fit to Xe–CH_4 and to Xe–CF_4 are slightly different, so that a common Xe–C shielding function may not be used.

Calculated shielding values at 70 (R,θ) points each for Xe–CO_2 and Xe–N_2 were fitted to the following functional form:

$$\{\sigma(R,\theta)-\sigma(\infty)\} = \sum_{p=6,\text{even}}^{12} R^{-p} \sum_{\lambda=0,\text{even}}^{6} a_{p\lambda} P_\lambda(\cos\theta), \quad (3)$$

where P_λ is a Legendre polynomial. For Xe–CO the values at 130 (R,θ) points were fitted to

$$\{\sigma(R,\theta)-\sigma(\infty)\} = \sum_{p=6,\text{even}}^{12} R^{-p} \sum_{\lambda=0}^{4} a_{p\lambda} P_\lambda(\cos\theta). \quad (4)$$

We use only even inverse powers of R for all cases, symmetrical and unsymmetrical, since the nucleus of interest resides in a molecule that has spherical symmetry.

RESULTS AND COMPARISONS WITH EXPERIMENT

Xe–CO_2

The shielding values calculated for Xe–N_2 using DFT/B3LYP have the same angular dependence as obtained previously using the Hartree–Fock method,[17] but the DFT values are much more deshielded at each (R,θ) configuration. We fitted the current results to Eq. (3). A good potential function is available for Xe–CO_2, based on crossed-molecular beam scattering cross sections, the best experimental data for refining those portions of the potential function close to r_0. The Xe–CO_2 potential function of Buck *et al.*[23] was fitted to crossed molecular beam differential energy loss spectra, including multiple collision rotational rainbows.[24] In our earlier work,[17] this potential has been found to reproduce fairly well the parameters obtained from the van der Waals spectral data, including bend and stretch frequencies and rotational constants of the dimer,[25,26] as well as the temperature-dependent mixture second virial coefficients.[27]

Using the Buck potential in Eq. (1) we calculated $\sigma_1(T)$ for Xe–CO_2 using both the Hartree–Fock and the DFT/B3LYP shielding surfaces. The results are analogous to the findings in the Xe–Xe case: the set of $\sigma_1(T)$ experimental values falls between the results calculated using the Hartree–Fock and the DFT/B3LYP shieldings. The experiment corresponds to 1.191 times the Hartree–Fock function or 0.8145 times the DFT shielding function. In the case of Xe–Xe the factors were 1.16 and 0.85, respectively. Figure 1(a) shows the comparison with experiments,[19] and in Fig. 1(b) we see the results of using $1.191\sigma_{\text{Hartree–Fock}}(R,\theta)$ and $0.8145\sigma_{\text{B3LYP}}(R,\theta)$ to calculate $\sigma_1(T)$. The agreement with experiment is excellent with either of the scaled functions. The deviations at the lowest temperatures may be due in part

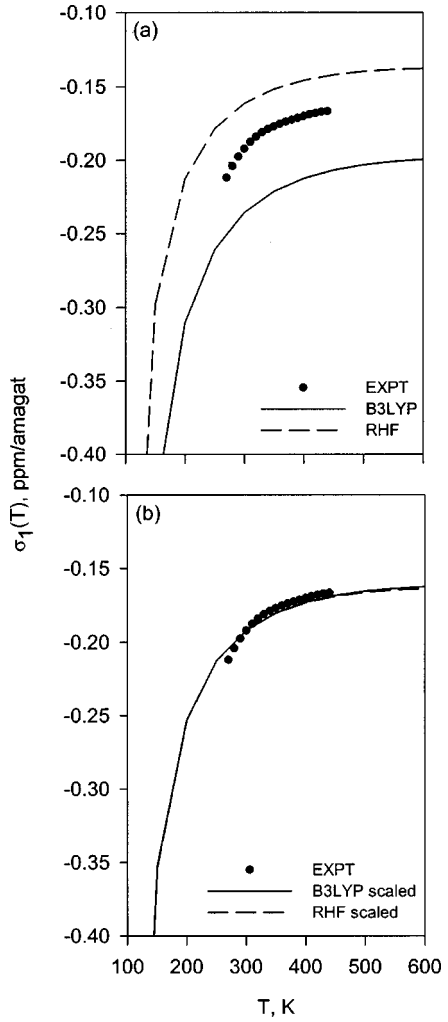

FIG. 1. Comparison of theoretical calculations with experimental $\sigma_1(T)$ for $Xe–CO_2$. Theoretical values at 50 K intervals are joined with straight lines in this figure and Fig. 2. (a) The $\sigma_1(T)_{Xe–CO_2}$ calculated using the B3LYP and the Hartree–Fock shielding response functions, and (b) using $1.19 \times \sigma_{Hartree–Fock}(R)$, and $0.81 \times \sigma_{B3LYP}(R)$ shielding functions. The Buck potential function for $Xe–CO_2$ was used in all calculations of the thermal averages.

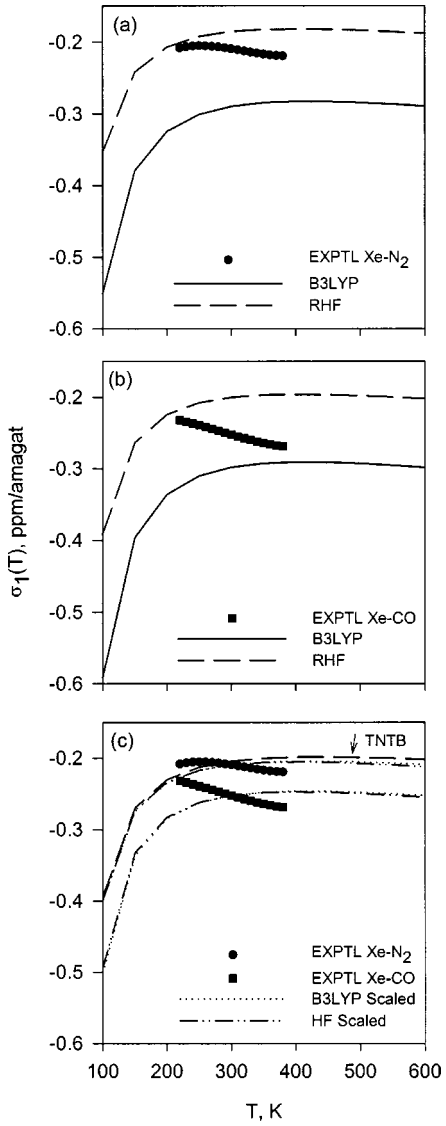

FIG. 2. Comparison of theoretical calculations with experimental density coefficients of the Xe shielding as a function of temperature, $\sigma_1(T)$ for $Xe–N_2$ and Xe–CO calculated using our Hartree–Fock–damped dispersion potential function: (a) the $\sigma_1(T)_{Xe–N_2}$ calculated using the B3LYP and the Hartree–Fock shielding response functions, and (b) the $\sigma_1(T)_{Xe–CO}$ calculated using the B3LYP and the Hartree–Fock shielding response functions, and (c) using $1.130 \times \sigma_{Hartree–Fock}(R)$, and $0.7238 \times \sigma_{B3LYP}(R)$ shielding functions for $Xe–N_2$ and using $1.262 \times \sigma_{Hartree–Fock}(R)$, and $0.8465 \times \sigma_{B3LYP}(R)$ shielding functions for Xe–CO. For comparison, the results for $Xe–N_2$ with the TNTB potential using the same shielding functions are also shown in (c).

to some contamination of the second virial coefficient of the Xe chemical shift with higher order contributions which are more significant at lower temperatures.

$Xe–N_2$

The DFT/B3LYP shielding in the $Xe–N_2$ system, like $Xe–CO_2$, is found to track the previously calculated Hartree–Fock shielding function.[17] The two shielding functions scale, so if we take 1.130 times the Hartree–Fock function or 0.7238 times the DFT shielding function, the two functions reproduce the room temperature value of the density coefficient for Xe in N_2 gas. The temperature dependence from the $\sigma_1(T)$ experiments suggests that the $Xe–N_2$ potential is highly anisotropic. This is in line with the known anisotropies of the $N_2–Ar$ and the $N_2–Kr$ potential surfaces that best agree with scattering, relaxation, and van der Waals spectral data.[28,29] A number of constructed potential functions, using the same dispersion coefficients from Hettema *et al.*[30] were tried in the present work, in addition to the ones reported previously.[17]

In Fig. 2(a) we see that the experimental data fall between the values calculated with and without electron correlation. These results were obtained by using our Hartree–Fock–damped dispersion potential function. This potential function had been constructed as described earlier,[17] with the dispersion coefficients from Hettema *et al.*[30] except that the entire dispersion part is enhanced by the factor 1.15 in order to obtain reasonably good agreement with the pressure virial coefficient $B_{12}(T)$. We find approximately the same fraction

of electron correlation corrections for Xe–N_2 that we had found for Xe–CO_2, that is, the Hartree–Fock functions are multiplied by the factor 1.130 and the B3LYP functions by the factor 0.7238 for Xe–N_2.

Xe–CO

The Xe shielding values obtained using DFT/B3LYP have the same angular dependence as obtained previously using the Hartree–Fock method.[17] For the same Xe–C as Xe–O distance in the collinear configuration, the shielding is much more pronounced when the Xe is approaching the C atom ($\theta=180°$) than the O atom ($\theta=0°$). We fitted the values obtained from the B3LYP/DFT calculations at the various configurations to Eq. (4).

There is a large difference between the repulsive potential energies in the Xe–OC and the Xe–CO configurations. At the global minimum (nearly 90° arrangement) of the van der Waals Xe(CO) complex, the average distance between the Xe and the center of mass of the CO is 4.195 Å.[31] The shielding surface reflects this same large anisotropy, already noted in the Hartree–Fock calculations. Calculated $\sigma_1(T)$ values are shown in Fig. 2(b) for Xe–CO. As for Xe–CO_2, we find that the Xe–CO system has a comparable fraction for electron correlation that needs to be added to the Hartree–Fock shielding function, that is, 1.262 times the Hartree–Fock shielding function and 0.8465 times the B3LYP/DFT shielding function. These are not very different from the Xe–N_2 and the Xe–CO_2 systems. The Hartree–Fock–damped dispersion potential function used here for Xe–CO, constructed as described in Ref. 17, needed an enhanced dispersion part (by a factor 1.18) in order to agree with the experimental temperature dependence of the pressure virial coefficients $B_{12}(T)$. The parameters of the Xe–CO_2, Xe–CO, and Xe–N_2 shielding and potential functions used here are given in supplementary materials.[32]

In previous work, using Hartree–Fock values for the shielding function $\sigma(R,\theta)$, we were unsuccessful in finding a potential function for Xe–N_2 that would predict the proper $\sigma_1(T)$ magnitude at 300 K and the correct temperature dependence, as well as reproducing the second pressure virial coefficient $B_{12}(T)$.[17] By scaling the dispersion so as to deepen the well to obtain better $B_{12}(T)$ values and magnitude of σ_1(300 K), the unusual temperature dependence (opposite to the usually observed sign of the temperature coefficient)[20] of $\sigma_1(T)$ was lost. The Hartree–Fock values of σ were not sufficiently deshielding. In the present study, with electron correlation included in the Xe shielding response surface $\sigma(R,\theta)$, an enhanced well depth in the potential does not have to be invoked to compensate for the $\sigma(R,\theta)$ deficiency, to lead to a magnitude of σ_1(300 K) closer to experiment. Nevertheless, the potential functions have yet to be found that will give the correct temperature dependence of the $\sigma_1(T)$ for Xe–N_2 and Xe–CO and which also give values of the second pressure virial coefficients $B_{12}(T)$ in good agreement with the experimental values.[27] Since the second pressure virial coefficient $B_{12}(T)$ is not very sensitive to the anisotropy of the potential we need primarily the correct volume of the potential well to calculate accurate $B_{12}(T)$ values. On the other hand, since we have found the shielding function to be highly deshielded at short distances and highly θ-dependent, we need the correct θ dependence of r_0 to obtain accurate density coefficients of the chemical shifts in the gas phase $\sigma_1(T)$. In Fig. 2(c) is a comparison of the calculated with the experimental density coefficients of the chemical shift for Xe in mixtures of Xe in CO and N_2 using the shielding functions with electron correlation, i.e., 1.130 and 1.262 times the Hartree–Fock shielding for Xe–N_2 and Xe–CO, respectively. The agreement achieved with the experimental data is only modest for both Xe–CO and Xe–N_2. We include the example of the TNTB potential function for Xe–N_2,[33] which provides the best $B_{12}(T)$ of those Xe–N_2 potentials used in earlier work,[17] to demonstrate that potential functions that reproduce the $B_{12}(T)$ generally fail to reproduce the temperature dependence of $\sigma_1(T)$ for Xe–N_2 and Xe–CO. We can construct potential functions for Xe–N_2 and Xe–CO that would reproduce the observed maximum and the pronounced experimental decrease in $\sigma_1(T)$ with increasing temperature, however these potential functions do not provide good agreement with second virial coefficients. In principle, all $\sigma_1(T)$ curves would exhibit a maximum (see, for example, Fig. 6 in Ref. 34), although for most gases we have not observed this maximum in the experimental temperature ranges studied.

Xe–CH_4

We fitted both the Hartree–Fock and the B3LYP/DFT shielding values calculated for various Xe–CH_4 configurations to the functional form of Eq. (2). For Xe–CH_4, there is a high quality potential function fitted to crossed molecular beam scattering data which can be adopted for the present work. The best available Xe–CH_4 potential function was fitted by Liuti *et al.* to crossed-molecular beam absolute integral cross sections, including analysis of the fully developed glory oscillations.[35] We had fitted this potential to Xe–C and Xe–H Maitland–Smith functions previously,[36] and used the latter successfully to reproduce the Xe chemical shifts and distributions of Xe and CH_4 molecules among the cages of crystalline zeolite NaA. The parameters for that Xe–CH_4 potential, used in the present work, are given in Table I.

In Figure 3(a) we compare the second virial coefficients of the Xe shielding $\sigma_1(T)$ calculated using the Xe–CH_4 shielding function used previously (scaled from Ar–CH_4),[36] and also the B3LYP and the Hartree–Fock calculations of the present work. The calculated density coefficients from the scaled shielding function are in very good agreement with the B3LYP results and with the experiments. The Hartree–Fock values give $\sigma_1(T)$ results that are too small. Thus, we can either continue to use the previous scaled version of Ref. 36 or else adopt the B3LYP shielding function for Xe–CH_4. We choose the latter. The coefficients of the Xe–C and Xe–H shielding functions used here for Xe–CH_4 are given in Table I.

Xe–CF_4

We fitted both the Hartree–Fock and the B3LYP/DFT shielding values calculated for various Xe–CF_4 configura-

TABLE I. Coefficients for site–site shielding functions Xe–C(H_4), Xe–C(F_4), Xe–H, Xe–F. as defined in Eq. (2). Also given are the parameters for the Maitland–Smith forms of Xe–C, Xe–H, Xe–F potential functions, and alternate parameters for exp-6 potential functions for Xe–C, Xe–H, Xe–F. The former are suitable for Monte Carlo simulations and the latter for molecular dynamics simulations.

Shielding function, ppm	Xe–C(H_4)	Xe–C(F_4)	Xe–H	Xe–F
$\{\sigma(R,\theta,\phi)-\sigma(\infty)\}_{CX_4}$ $=\sum_{p=6,\text{even}}^{12} c_p R_{XeC}^{-p}+\sum_{i=1}^{4}\sum_{p=6,\text{even}}^{12} x_p R_{Xei}^{-p}$	c_6 Å^{-6} $=1.482\,11\times10^5$ c_8 Å^{-8} $=-1.045\,90\times10^7$ c_{10} Å^{-10} $=1.901\,32\times10^8$ c_{12} Å^{-12} $=-1.384\,33\times10^9$ c_{14} Å^{-14} $=3.455\,61\times10^9$	c_6 Å^{-6} $=1.628\,91\times10^4$ c_8 Å^{-8} $=-2.909\,18\times10^6$ c_{10} Å^{-10} $=4.835\,19\times10^7$ c_{12} Å^{-12} $=-2.760\,70\times10^8$ c_{14} Å^{-14} $=5.230\,79\times10^8$	h_6 Å^{-6} $=-8.583\,34\times10^3$ h_8 Å^{-8} $=6.557\,33\times10^5$ h_{10} Å^{-10} $=-1.421\,31\times10^7$ h_{12} Å^{-12} $=6.347\,47\times10^7$ h_{14} Å^{-14} $=-4.200\,88\times10^7$	f_6 Å^{-6} $=-7.445\,68\times10^3$ f_8 Å^{-8} $=6.937\,67\times10^5$ f_{10} Å^{-10} $=-1.899\,30\times10^7$ f_{12} Å^{-12} $=1.321\,48\times10^8$ f_{14} Å^{-14} $=-2.776\,10\times10^8$
Potential function: $V(\text{Xe–CX}_4)$ $=V(R_{XeC})+\Sigma_i^4 V(R_{XeXi})$	Xe–C(H_4)	Xe–C(F_4)	Xe–H	Xe–F
$V(R_{XeA})=\varepsilon\left\{\left(\frac{6}{n-6}\right)\bar{r}^{-n}-\left(\frac{n}{n-6}\right)\bar{r}^{-6}\right\}$	$\varepsilon/k_B=141.52$ K $m=13$ $\gamma=9.5$ $r_{min}=4.0047$ Å	$\varepsilon/k_B=141.52$ K $m=13$ $\gamma=9.5$ $r_{min}=4.0047$ Å	$\varepsilon/k_B=53.07$ K $m=13$ $\gamma=9.5$ $r_{min}=3.671$ Å	$\varepsilon/k_B=78.235$ K $m=13$ $\gamma=9.5$ $r_{min}=3.941$ Å
$\bar{r}=\frac{R_{XeA}}{r_{min}}$, $n=m+\gamma(\bar{r}-1)$				
Alternative $V(R_{XeA})$ $=\varepsilon\left[\frac{6}{\alpha-6}\exp^{[\alpha(1-(R_{XeA}/r_{min}))]}-\frac{\alpha}{\alpha-6}\left(\frac{r_{min}}{R_{XeA}}\right)^6\right]$	$\varepsilon/k_B=141.2$ K $\alpha=16.1$ $r_{min}=3.99$ Å	$\varepsilon/k_B=141.2$ K $\alpha=16.1$ $r_{min}=3.99$ Å	$\varepsilon/k_B=53.3$ K $\alpha=15.9$ $r_{min}=3.66$ Å	$\varepsilon/k_B=78.5$ K $\alpha=14.2$ $r_{min}=3.93$ Å

tions to the functional form of Eq. (2). Just as in the Xe–CH_4 system, the calculations including electron correlation, albeit using approximate functionals, produce shielding responses that are significantly more deshielded than using the Hartree–Fock method. For the Xe–CF_4 chemical shifts, we will assume that the electron correlation for Xe–CF_4 is about the same fraction as for Xe–CH_4. That is, we will use the site–site shielding functions fitted to the B3LYP calculations for Xe–CF_4 as the final shielding functions to be used to interpret the gas phase chemical shifts of Xe dilute in mixtures with various densities of CF_4 gas.

For Xe–CF_4, we need similar Xe–C and Xe–F Maitland–Smith functions as we have used for Xe–CH_4, which will reproduce the experimental values of the chemical shifts in the gas phase mixture. As a starting point for a Xe–CF_4 potential in the form of pairwise additive site–site Xe–C and Xe–F potentials, we use the same Xe–C parameters as was found for Xe–CH_4 and find the ε and r_{min} of the Xe–F by using as starting point the Xe–Ne potential.[37] For Xe–F we use $r_{min}=3.93$ Å (somewhat longer than the 3.861 Å for Xe–Ne) and $\varepsilon/k_B=78.5$ K (slightly deeper than 74.205 K for Xe–Ne). We refined the Xe–F potential parameters to make the temperature dependence of the density coefficients agree with experiment in the region of interest (280 to 420 K) for Xe–CF_4. The results are shown in Fig. 3(b). The parameters for the Xe–CF_4 potential used here are given in Table I. Isotropic two-center Xe–CF_4 potentials previously used by others cannot be used in the present work if the results are to be adopted for understanding the chemical shifts of Xe dissolved in liquid perfluoroalkanes.

Our calculations are in excellent agreement with experiment in terms of the relative magnitudes of the average shielding response from CF_4 (smaller average response) compared to that from CH_4, despite the larger polarizability of CF_4 in comparison to CH_4 molecule. This greater average response from CH_4 arises from two contributing factors which are illustrated in Fig. 4: One is the more pronounced intrinsic Xe shielding response for CH_4 compared to CF_4, for comparable configurations of the Xe–CX_4 supermolecule. A second factor is that the longer C–F (compared to C–H) bond corresponds to averages at longer distances for the Xe–C shielding contribution; and the longer r_{min} for the Xe–F (compared to Xe–H) potential function corresponds to averages at longer distances for the Xe–F shielding contribution. The intrinsic shielding response and the potential energy function along each of three particular Xe approaches to CH_4 and CF_4 are shown in Fig. 4. We see that for all approaches (except for the approach along the C–X bond), the intrinsic shielding response is more pronounced for Xe–CH_4 than for Xe–CF_4 at the same Xe–C distance. At the same time, the favorable potential energy is at longer Xe–C distances for Xe–CF_4 than for Xe–CH_4. Since the intrinsic shielding response falls off drastically with increasing distance, the averages are smaller for CF_4 than for CH_4 at the same temperature. Figure 4 clearly shows that the contribution to the total integral from each of the three approaches is a larger negative value for Xe–CH_4 than for Xe–CF_4. The

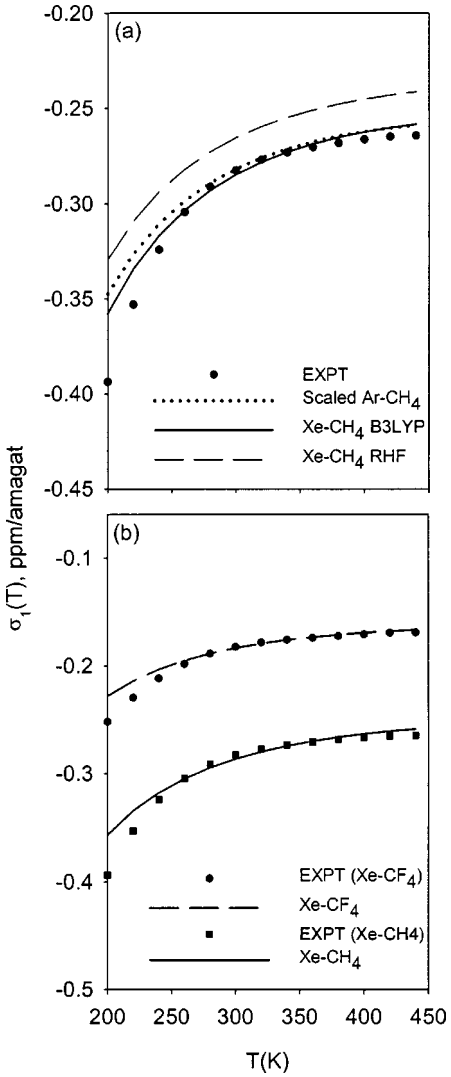

FIG. 3. Comparison with experimental density coefficients of the Xe shielding as a function of temperature: $\sigma_1(T)$ for Xe–CH_4 and Xe–CF_4. (a) The dotted curve is the $\sigma_1(T)$ previously calculated using the shielding function scaled from Ar–CH_4, the solid and dashed curves used shielding values from density functional (B3LYP) and Hartree–Fock calculations, respectively. (b) The comparison of $\sigma_1(T)$ for Xe–CH_4 and Xe–CF_4. The Xe shielding functions used were based on the density functional (B3LYP) values for both Xe–CH_4 and Xe–CF_4 systems. The same potential functions were used to calculate all $\sigma_1(T)$ for Xe–CH_4 in (a) and (b). The potential function parameters for Xe–CH_4 and Xe–CF_4 are given in Table I.

parameters for the Xe–C and Xe–F shielding function used here for Xe–CF_4 are given in Table I.

CONCLUSIONS

Since the Xe–CO_2 and Xe–CH_4 potentials are adequate, we used the experimental $\sigma_1(T)$ to find that the electron correlation contributions in Xe–CO_2 are very similar to the fraction found in Xe–Xe, and we found that we can use the B3LYP shielding values for σ(Xe–CH_4). For Xe–CF_4 no well-tested potential function was available, so we used B3LYP shielding values for σ(Xe–CF_4) to find Xe–F site–site potential parameters that provided good agreement with the experimental second virial coefficient for chemical shifts in Xe–CF_4 mixtures.

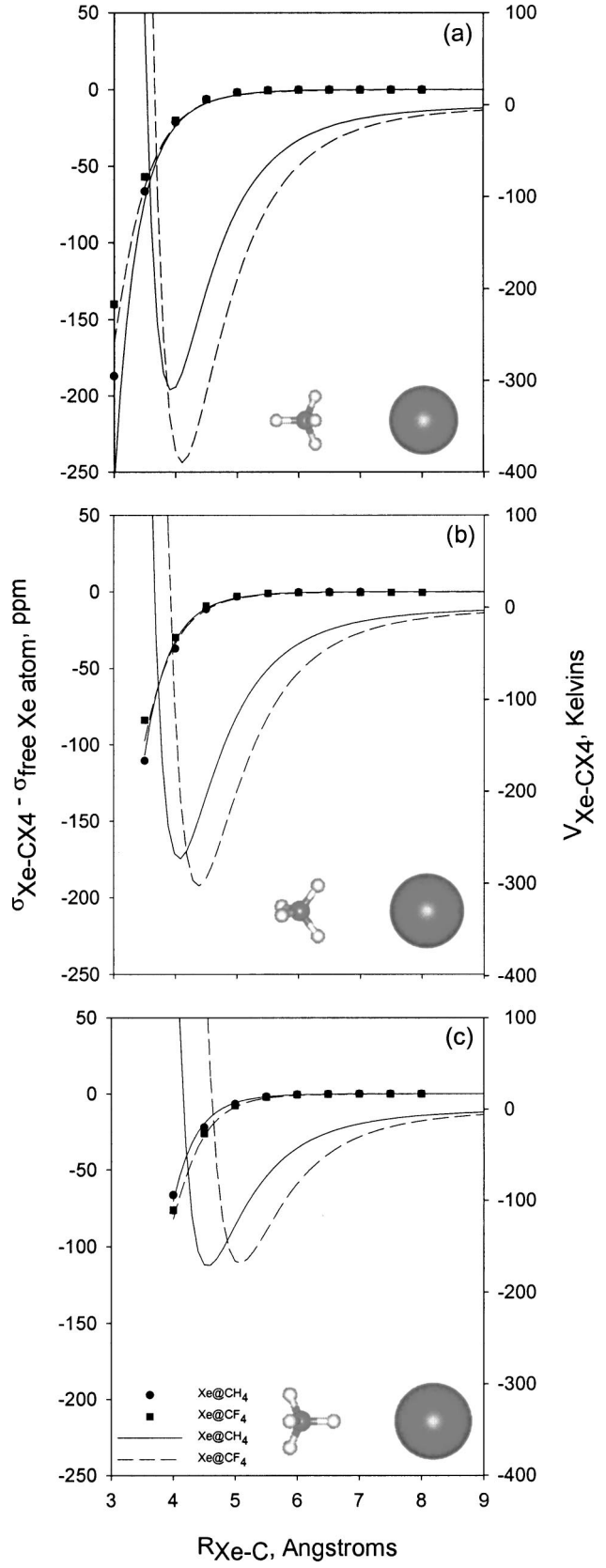

FIG. 4. Comparisons of the calculated intrinsic Xe shielding responses for a specific direction of approach of Xe toward the CH_4 and CF_4 molecules and the potential energy function along this trajectory. (a) Xe approach perpendicular to the triangular face of H_3 or F_3, (b) Xe approach perpendicular to the edge of the tetrahedron, along the bisector of the HCH or FCF bond angle, (c) Xe approach along a vertex of the tetrahedron toward the H–C or F–C bond.

Earlier approximate Xe–N_2 and Xe–CO potentials were inadequate to provide the correct temperature dependence of the gas phase experiments. We report a set of Xe–N_2 and Xe–CO potentials that provide values in reasonably good agreement with both the pressure virial coefficient $B_{12}(T)$ and the room temperature Xe NMR experiments in gas mixtures. We find the B3LYP and Hartree–Fock shielding functions to be scalable to each other in each of the systems Xe–CO_2, Xe–N_2, and Xe–CO, both B3LYP and Hartree–Fock providing a good description of the anisotropy of the Xe shielding response. Furthermore, the fraction of electron correlation contributions to the Xe shielding response appears to be about the same for CO, N_2, and CO_2, i.e., 13%–26% of the total shielding. The potential and shielding functions found here can be used for competitive adsorption simulations for Xe–N_2, Xe–CO, and Xe–CO_2 mixtures in zeolites, in which detailed experimental data is available for the individual chemical shifts of $Xe_n(N_2)_{\langle m\rangle}$ or $Xe_n(CO)_{\langle m\rangle}$ or $Xe_n(CO_2)_{\langle m\rangle}$ in a cavity, where $n=1-6$, for variable $\langle m\rangle$.[38]

We have constructed shielding surfaces and potential functions, which have been tested against gas phase chemical shift data, for applications to molecular dynamics averaging of Xe chemical shifts in liquid solvents containing CH_3, CH_2, CH, CF_3, CF_2, and CF groups. Potential functions that are to be used for averaging Xe chemical shifts must have a better repulsive part than is provided by Lennard-Jones because the shielding function makes very large contributions at short distances. Thus, we recommend potential functions of the Maitland–Smith form, suitable for Monte Carlo simulations, and exp-6 form suitable for MD simulations. Both forms have been found to give good agreement with experimental chemical shifts in gas mixtures. The Xe–C, Xe–F, Xe–H potential functions and shielding functions provided here (in Table I) can be used for molecular dynamics simulations of solutions of Xe in liquid *n*- or branched alkanes and perfluoroalkanes to provide Xe chemical shifts in solutions. Other possible applications are for hydrophobic pockets or channels that have primarily CH_n or CF_n functional groups lining the walls, such as in polymer voids. Examples are Xe in the microvoids of polymer membranes such as poly(4-methylpentene-1)$-(CH_2-CRH)_n$ where $R=CH_2CH(CH_3)_2$ (PMP),[39] polyisobutylene $-(CH_2-CR_2)_n$ where $R=CH_3$ (PIB),[40] and various high or low density forms of polyethylene $-(CH_2-CH_2)_n-$(PE),[41] and poly(tetrafluoroethylene) $-(CF_2-CF_2)_n-$(TFE).

ACKNOWLEDGMENT

This research was funded by the National Science Foundation (Grant No. CHE-9979259).

[1] T. R. Stengle, S. M. Hosseini, H. G. Basiri, and K. L. Williamson, J. Solution Chem. **13**, 779 (1984).
[2] P. Diehl, R. Ugolini, N. Suryaprakash, and J. Jokisaari, Magn. Reson. Chem. **29**, 1163 (1991).
[3] J. L. Bonardet, J. Fraissard, A. Gedeon, and M. A. Springuel-Huet, Catal. Rev. - Sci. Eng. **41**, 115 (1999).
[4] Y. Wang, P. T. Inglefield, and A. A. Jones, Polymer **43**, 1867 (2002).
[5] D. T. Bong, T. D. Clark, J. R. Granja, and M. R. Ghadiri, Angew. Chem., Int. Ed. Engl. **40**, 988 (2001).
[6] C. H. Görbitz, Acta Crystallogr., Sect. B: Struct. Sci. **B58**, 849 (2002).
[7] A. Cherubini and A. Bifone, Prog. Nucl. Magn. Reson. Spectrosc. **42**, 1 (2003).
[8] H. E. Möller, M. S. Chawla, X. J. Chen, B. Driehuys, L. E. Hedlund, C. T. Wheeler, and G. A. Johnson, Magn. Reson. Med. **41**, 1058 (1999).
[9] A. Bifone, Y. Q. Song, R. Seydoux, R. E. Taylor, B. M. Goodson, T. Pietrass, T. F. Budinger, G. Navon, and A. Pines, Proc. Natl. Acad. Sci. U.S.A. **93**, 12932 (1996).
[10] C. I. Ratcliffe, Annu. Rep. NMR Spectrosc. **36**, 123 (1998).
[11] D. Stueber and C. J. Jameson, J. Chem. Phys. **120**, 1560 (2004).
[12] J. A. Ripmeester, C. I. Ratcliffe, and J. S. Tse, J. Chem. Soc., Faraday Trans. 1 **84**, 3731 (1988).
[13] J. A. Ripmeester and C. I. Ratcliffe, J. Phys. Chem. **94**, 8773 (1990).
[14] K. A. Udachin, G. D. Enright, C. I. Ratcliffe, and J. A. Ripmeester, J. Am. Chem. Soc. **119**, 11481 (1997).
[15] C. J. Jameson and S. Murad, Chem. Phys. Lett. **380**, 556 (2003).
[16] C. J. Jameson, D. N. Sears, and S. Murad (unpublished).
[17] A. C. de Dios and C. J. Jameson, J. Chem. Phys. **107**, 4253 (1997).
[18] C. J. Jameson, A. K. Jameson, and S. M. Cohen, J. Chem. Phys. **65**, 3401 (1976).
[19] C. J. Jameson, A. K. Jameson, and S. M. Cohen, J. Chem. Phys. **66**, 5226 (1977).
[20] C. J. Jameson, A. K. Jameson, and H. Parker, J. Chem. Phys. **68**, 3943 (1978).
[21] H. Partridge and K. Faegri, Jr., NASA Tech. Memo. 103918 (1992).
[22] D. A. Bishop and S. M. Cybulski, Chem. Phys. Lett. **211**, 255 (1993).
[23] U. Buck, F. Huisken, D. Otten, and R. Schinke, Chem. Phys. Lett. **101**, 126 (1983).
[24] U. Buck, D. Otten, R. Schinke, and D. Poppe, J. Chem. Phys. **82**, 202 (1985).
[25] M. Iida, Y. Ohshima, and Y. Endo, J. Phys. Chem. **97**, 357 (1993).
[26] R. W. Randall, M. A. Walsh, and B. J. Howard, Faraday Discuss. Chem. Soc. **85**, 13 (1988).
[27] J. Brewer, Determination of Mixed Virial Coefficients, Tech. Report AADD 663448, AFOSR No. 67-2795, Air Force Office of Scientific Research, Arlington, VA, 1967.
[28] L. Beneventi, P. Casavecchia, G. G. Volpi, C. C. K. Wong, and F. R. W. McCourt, J. Chem. Phys. **98**, 7926 (1993).
[29] F. R. W. McCourt, M. A. ter Horst, and C. J. Jameson, J. Chem. Phys. **102**, 5752 (1995).
[30] H. Hettema, P. E. S. Wormer, and A. J. Thakkar, Mol. Phys. **80**, 533 (1993).
[31] J. W. C. Johns, Z. Lu, and A. R. W. McKellar, J. Mol. Spectrosc. **159**, 210 (1993).
[32] See EPAPS document No. E-JCPSA6-121-318425 for tables of shielding response functions and potential functions used here for Xe–CO_2, Xe–CO, and Xe–N_2. A direct link to this document may be found in the online article's HTML reference section. The document may also be reached via the EPAPS homepage (http://www.aip.org/pubservs/epaps.html) or from ftp.aip.org in the directory /epaps/. See the EPAPS homepage for more information.
[33] M. A. ter Horst, Ph.D. thesis, University of Illinois at Chicago, 1993.
[34] C. J. Jameson and A. C. de Dios, J. Chem. Phys. **97**, 417 (1992).
[35] G. Liuti, F. Pirani, U. Buck, and B. Schmidt, Chem. Phys. **126**, 1 (1988).
[36] C. J. Jameson, A. K. Jameson, P. Kostikin, and B. I. Baello, J. Chem. Phys. **112**, 323 (2000).
[37] D. A. Barrow, M. J. Slaman, and R. A. Aziz, J. Chem. Phys. **91**, 6348 (1989).
[38] D. N. Sears, C. J. Jameson, and A. K. Jameson (unpublished).
[39] H. Yoshimizu, H. Fukatsu, T. Suzuki, Y. Tsujita, and T. Kinoshita, Polymer **30**, 981 (1998).
[40] J. B. Miller, J. H. Walton, and C. M. Roland, Macromolecules **26**, 5602 (1993).
[41] A. P. M. Kentgens, H. A. van Boxtel, R. J. Verweel, and W. S. Veeman, Macromolecules **24**, 3712 (1991).